J|A|C|S
COMMUNICATIONS

Published on Web 06/03/2008

Chelation of a Proton by an Aliphatic Tertiary Diamine

Sepideh Yaghmaei, Sevana Khodagholian, J. Michael Kaiser, Fook S. Tham, Leonard J. Mueller, and Thomas Hellman Morton*

Department of Chemistry, University of California, Riverside, California 92521-0403

Received March 17, 2008; E-mail: morton@citrus.ucr.edu

Hydrogen bonding embraces a variety of attractive interactions at the molecular level. Strong hydrogen bonding refers to cases where one of the partners bears an electrical charge: either the hydrogen bond acceptor is an anion or the donor is a cation. Bifluoride ion (FHF^-) represents a well-known instance of the former, while the Zundel ion ($H_2O^{\bullet\bullet\bullet}HOH_2^+$) represents an example of the latter. In both of these ions, theory and gas phase experiments support the inference that the potential energy surfaces exhibit minima at which the bridging proton lies midway between the heteroatoms.[1,2]

Published studies of the proton-bound dimer of ammonia ($H_3N^{\bullet\bullet\bullet}HNH_3^+$) present a less clear-cut picture.[3] Theory and recent gas phase infrared spectra suggest that the bridging proton must traverse a potential energy maximum in order to transit from one nitrogen to the other. Nevertheless, the height of this central barrier may be so low that the zero-point level lies near the barrier top. As a consequence, the lowest energy vibrational wavefunction can achieve its maximum value at the midpoint, even though this corresponds to a local maximum in the potential. This communication reports an experimental demonstration of a case where a proton bridging between two chemically equivalent tertiary amino groups sits midway between the two nitrogens.

Recent interest in "encircled protons" raises the question as to the conditions under which a proton becomes symmetrically chelated in positive ions.[4] The literature contains a number of examples where such geometries seem plausible,[5] but empirical validation has thus far proven elusive. Data presented here deal with an internally proton-bridged tertiary diaminium ion, in which the NHN bond angle is nearly linear. As in the case of primary diaminium ions[6] and $H_3N^{\bullet\bullet\bullet}HNH_3^+$, theory predicts a central barrier. A combination of X-ray crystallography and solid phase NMR, described below, shows that the proton lies at the midpoint in its equilibrium position. This contrasts with the conjugate acid ions of "proton sponges", where the NHN bond angle is $\leq 162°$ and the hydrogen transits back and forth between the nitrogens.[7]

The motifs that crystalline monoprotonated aliphatic diamine salts can adopt include the three hydrogen bonding patterns drawn in Scheme 1: salt-bridged (i.e., where the hydrogen bond donor and acceptor carry opposite charges), clustered, or cyclic (where A^- symbolizes a negatively charged counterion).

Chart 1 illustrates examples of these three categories. Monoprotonated *cis*-1,5-cyclooctanediamine[8] forms a 1:1 triflate salt, **1**, that crystallizes in the salt-bridged motif, where the eight-membered ring adopts a crown (or chair−chair) conformation having both amino groups equatorial, with intermolecular $NH^{\bullet\bullet\bullet}N$ strong hydrogen bonds in addition to the salt bridge.

Crystallization of tertiary diamines in the clustered or cyclic motifs requires that proton bridging between nitrogens prevail over hydrogen bonds between protonated amino groups and the anion. In linear aliphatic tertiary diamines, the observed motif depends on the alkyl chain. The 1:1 triflate salt of monoprotonated *N,N,N′,N′*-

Scheme 1. Hydrogen Bonding Motifs of Monoprotonated Diamines

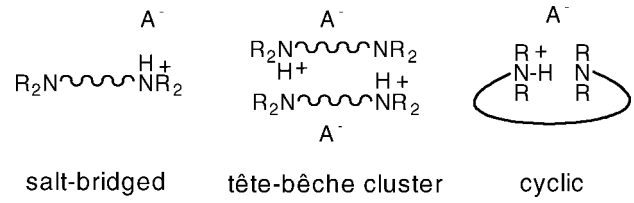

Chart 1. Monoprotonated Diamine Salts

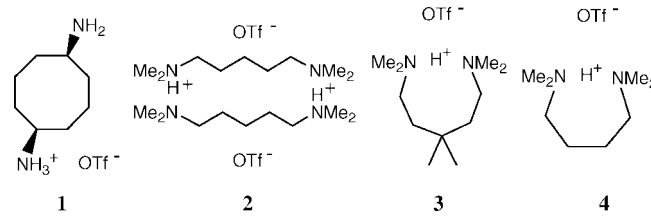

tetramethylcadaverine, $Me_2N(CH_2)_5NMe_2$, **2**, forms a dimeric cluster in a tête-bêche orientation. *gem*-Dimethyl substitution at position 3 of the 5-carbon chain leads to crystallization in the cyclic motif, as structure **3** represents.

Figure 1 summarizes the X-ray structures of **1** and **2**. Like **3**, the 1:1 triflate salt of monoprotonated *N,N,N′,N′*-tetramethylputrescine, $Me_2N(CH_2)_4NMe_2$, **4**, also crystallizes as an internally strong hydrogen-bonded structure, with the counterion situated at least 4 Å away from the bridging proton, as Figure 2 depicts. In contrast to **4**, which has two molecules per unit cell that are equivalent by symmetry, **3** has eight molecules per unit cell, possessing two slightly different conformations. For this reason, **4** was chosen for further study.

Previous experimental studies[9] provide evidence that strong hydrogen bonds prefer near linear geometries. X-ray crystallography does not provide a definitive picture of the location of the bridging proton in the monoprotonated diamine salts, but the electron density map indicates that the NHN bond angle in **4** is $\geq 172°$, consistent

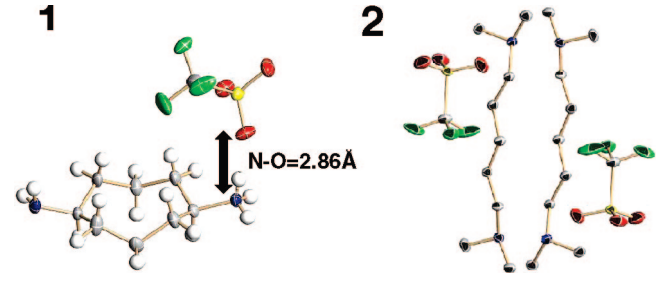

Figure 1. X-ray structure (50% thermal ellipsoids) of *cis*-1,5-cyclooctanediaminium monotriflate (**1**) and *N,N,N′,N′*-tetramethyl-cadaverinium monotriflate (**2**). Blue atoms symbolize nitrogen, green, fluorine; red, oxygen; and yellow, sulfur. Hydrogens not shown for structure **2**.

10.1021/ja8018725 CCC: $40.75

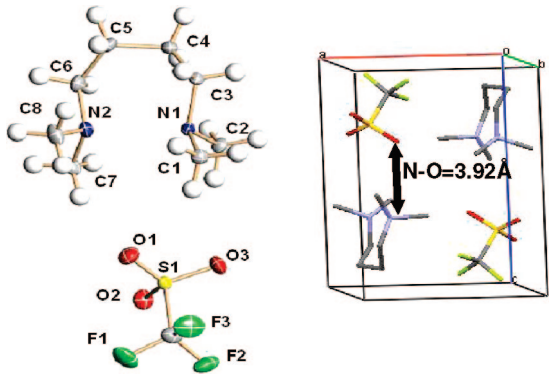

Figure 2. X-ray structure of *N*,*N*,*N*′,*N*′-tetramethylputrescinium monotriflate, **4** (left; 50% thermal ellipsoids), and its corresponding triclinic unit cell (right). The hydrogen between N^1 and N^2 is not shown.

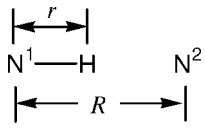

Figure 3. Coordinates used to describe the transit of a proton between two nitrogens, in which r and R represent scalar NH and NN distances. The symmetry coordinate corresponds to $(N^1H-N^2H)/\sqrt{2} = (R - 2r)/\sqrt{2}$.

with theoretical calculations on the gaseous monoprotonated cation in the absence of counterion.

The X-ray structure of the cyclic, monoprotonated triflate salt of $Me_2N(CH_2)_4NMe_2$, **4**, displays an internal N−N distance of R = 2.66 Å. The triflate oxygens lie more than 4 Å away from the mid-point between the nitrogen atoms, implying that salt bridging does not occur here. There is one anion per cation.

The d_{20}-analogue of **4** was also prepared, in which every hydrogen is substituted by deuterium except for the bridging proton. X-ray diffraction of a single crystal of **4**-d_{20} reveals the same geometry of the cation and anion as found for undeuterated **4**. Figure 3 summarizes the coordinate system used to describe the transit of the bridging proton from one nitrogen to the other.

Figure 4 illustrates calculated 1-dimensional potentials for the asymmetric stretch of the bridging proton in *N*,*N*,*N*′,*N*′-tetramethylputrescine (**4** without counterion or solvent), with zero-point vibrational wave functions computed using the following assumptions: (1) the NHN bond angle taken to be 180°; (2) the NN distance fixed at the value calculated for the optimized equilibrium geometry; and (3) calculated points fitted to a quartic/quadratic potential $V(x)$ as a function of the symmetry coordinate $x = (R - 2r)/\sqrt{2}$. The optimized stationary points have NHN bond angles slightly less than 180°, and the NN distance does change as the proton moves. A 4-dimensional potential surface takes those considerations into account (as discussed below) but does not give an average NH distance substantially different from the 1-dimensional pictures summarized in Figure 4.

Average values of the NH distance, $\bar{r}$, for 1-dimensional potentials were extracted from the zero point vibrational wave functions by calculating expectation values for $<1/r^3>$, a value that can be determined experimentally by measuring the $^{15}N-H$ dipolar coupling constant, $D_{15_{N-H}}$. Predicted values of $\bar{r}$ exhibit a degree of sensitivity that permits an NMR experiment to test various models.

Distances determined by crystallography correspond to the expectation values $<r>$ and $<R>$. Predicted values for the NH distance $<r>$ range from 1.41 Å when the barrier is much higher

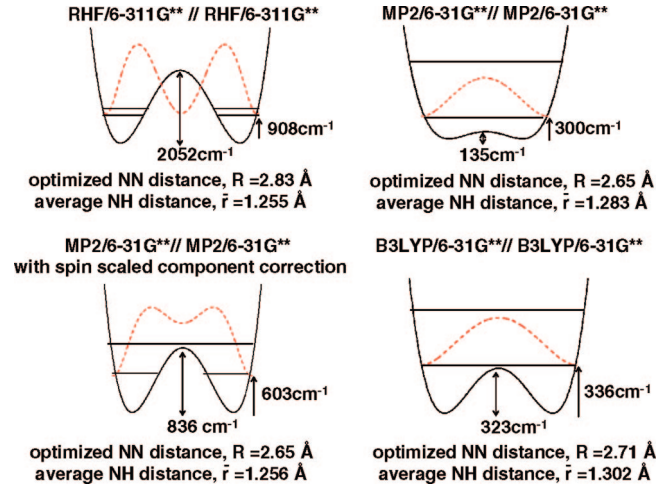

Figure 4. One-dimensional potential energy curves for the asymmetric stretching motion of a proton between the two nitrogens of an isolated *N*,*N*,*N*′,*N*′-tetramethylputrescinium ion, showing energy levels for the first and second vibrational states as well as the zero-point vibrational wave function (in dashed red). The x-axes correspond to the symmetry coordinate $(N^1H-N^2H)/\sqrt{2}$.

than the zero-point energy (as in the RHF potential) to 1.32 Å when the barrier is much lower (as in the MP2 potential without spin component scaled corrections). Inclusion of diffuse functions in the basis set does not substantially affect either the equilibrium geometry or the barrier height. Correction of the energies of MP2/6-31G** optimized geometries for spin components[10] gives an energy barrier between the two extremes, in which only the zero point level lies below the barrier top. X-ray structures do not situate the bridging proton well enough to differentiate among the options shown in Figure 4. Hence, this report relies upon a comparison of $D_{15_{N-H}}$ with the predicted values of $\bar{r}$ instead.

Crystalline **4** and its deuterated analogues were selected for solid phase NMR studies. The bridging proton of **4** is shifted considerably downfield from the CH resonances. The d_{16}-analogue of **4**, in which the methyl groups and the methyenes attached to nitrogen were replaced by deuterium, shows the NHN resonance to be 13 ppm downfield from the chemically equivalent CH_2 groups. The ^{15}N NMR shows the nitrogens to be equivalent.

Dipolar couplings between spin 1/2 nuclei have seen extensive use in measuring bondlengths.[11] They have proven especially helpful in determining hydrogen-bond distances in ionic solids.[12] In **4** the $^{15}N-^{1}H$ dipolar coupling was measured by natural abundance ^{15}N solid-state NMR techniques at room temperature, using Herzfeld and Berger's method[13] to analyze the spinning sideband manifold in the absence of proton decoupling, as Figure 5 portrays. Because the CHs were found to complicate data acquisition and analysis, the results below are reported for the d_{20}-analogue, in which there is only one proton coupled to nitrogen.

The asymmetry in the spinning sidebands is due to the tensorial combination of the ^{15}N chemical shift anisotropy (CSA) and the $^{15}N-^{1}H$ dipolar coupling.[14] The ^{15}N CSA tensor was independently measured under static cross-polarization (CP) conditions to have an anisotropy of $\eta = -473 \pm 16$ Hz and an asymmetry of $\eta = 0.70 \pm 0.07$ (all errors are 95% confidence intervals), corresponding to principal components of the chemical shift tensor $\mathbf{R}_{xx} = 46.0 \pm 0.8$, $\mathbf{R}_{yy} = 37.8 \pm 0.8$, and $\mathbf{R}_{zz} = 24.2 \pm 0.8$ ppm. These parameters were used in the analysis of the spinning sidebands in Figure 5. To fit the dipolar coupling a grid of spinning sideband intensities for the combination of the measured CSA values and dipolar coupling ranging from 50 to 8000 Hz and (grid spacing of 50 Hz)

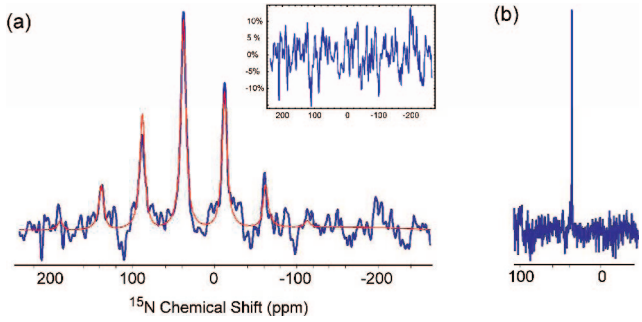

Figure 5. ^{15}N Natural abundance solid state NMR of **4**-d_{20} acquired at 9.4 T under conditions of cross polarization with magic angle spinning (a) without and (b) with 80 kHz ^{1}H decoupling. The experimental progression of sidebands in panel a is reproduced in blue, with the fitted curve in red superimposed upon it; the inset shows residuals from this fit.

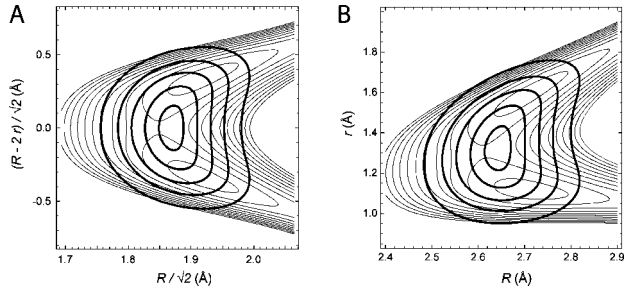

Figure 6. The 2-dimensional DFT potential surtace for H^+ transit between the nitrogens of *N*,*N*,*N*′,*N*′-tetramethylputrescine (gray countour plots): (A) as a function of the symmetry coordinates and (B) as a function of *r* and *R*. Zero-point wave functions are superimposed as black contour plots, spaced at 20%, 40%, 60%, 80%, and 95% of the maximum amplitude.

was generated. A least-squares fit gives a dipolar coupling constant of $D_{15_{N-H}} = 5250 \pm 90$ Hz. As the anisotropy is relatively small compared to the dipolar coupling, the sideband manifold was found to be essentially insensitive to the relative orientation of the CSA and dipolar tensors. The experimental value of $D_{15_{N-H}}$ corresponds to an average NH distance of 1.324 ± 0.008 Å.

Of the curves illustrated in Figure 4, the B3LYP/6-31G** potential gives the best fit to the experimental data. A 4-dimensional potential surface for motion of the bridging proton was constructed using DFT-calculated points for the symmetric and asymmetric stretching motions plus harmonic potentials for the in-plane and out-of-plane NHN bends from DFT normal modes.

Figure 6 depicts the anharmonic 2-dimensional part of the potential. The expectation value for the N−N distance, $<R>$, has a value of 2.655 Å, in good agreement with the X-ray value. For the 4-dimensional potential, where the NHN bond deviates from linearity, the predicted expectation value of $D_{15_{N-H}}$ becomes proportional to $<P_2(\cos\theta)/r^3>$, where θ designates the angle made by the NH bond with respect to its equilibrium orientation.[15] The two bending modes contribute to both the distance and the angular averaging of the coupling, giving an average NH distance of 1.322 Å, while $<r>$ has value of 1.327 Å. These theoretical predictions agree well with the experimental average NH distance inferred from the value of the $D_{15_{N-H}}$. The 1-dimensional DFT potential in Figure 4 makes a prediction not far from this, because shortening of *R* at the barrier top compensates for the lengthening of *r* as a consequence of the perpendicular NHN bending motions.

As the contours of the wave function plotted in Figure 6 indicate, the bridging proton in **4** experiences large amplitude motions, even in its zero point level. Nevertheless, its most probable position resides very near a potential energy maximum. This brings to mind the classical paradox of a creature, both hungry and thirsty, who remains immobile between food and drink, being unable to decide which to choose.[16] That image, known in philosophical circles as Buridan's Ass, describes an intriguing aspect of low barrier hydrogen bonds.[17] Further implications are the focus of current investigations.

Acknowledgment. The authors are grateful to Dr. Luke Daemen, Professors E. L. Chronister, Anne B. McCoy, and D. K. Glidden for material and advice. This work was supported by the Petroleum Research Fund of the American Chemical Society (T.H.M.), NSF Grants CHE0316551 (T.H.M) and CHE0349345 (L.J.M), and NIH Grant S10RR023677 (L.J.M).

Supporting Information Available: Crystallographic data for **1**−**4** and **4**-d_{20}; static ^{15}N CSA spectrum and fit. This material is available free of charge via the Internet at http://pubs.acs.org.

References

(1) (a) Kawaguchi, K.; Hirota, E. *J. Chem. Phys.* **1987**, *87*, 6838–6841. (b) Kawaguchi, K.; Hirota, E. *J. Mol. Struct.* **1995**, *352/353*, 389–394.
(2) Hammer, N. I.; Diken, E. G.; Roscioli, J. R.; Johnson, M. A.; Myshakin, E. M.; Jordan, K. D.; McCoy, A. B.; Huang, X.; Bowman, J. M.; Carter, S. *J. Chem. Phys.* **2005**, *122*, 244301. (b) Niedner-Schatteburg, G. *Angew. Chem., Int. Ed.* **2008**, *47*, 1008–1031.
(3) (a) Lutz, H. D.; Alici, E.; Henning, J.; Berthold, H. J.; Vonholdt, E. *J. Mol. Struct.* **1990**, *220*, 119–127. (b) Berthold, H. J.; Vonholdt, E.; Wartchow, R.; Vogt, T. *Zeitschr Kristall.* **1992**, *200*, 225–235. (c) Berthold, H. J.; Vonholdt, E.; Wartchow, R.; Vogt, T. *Zeitschr. Kristall.* **1993**, *203*, 199–214. (d) Schwarz, H. A. *J. Chem. Phys.* **1980**, *72*, 284–287. (e) Asmis, K. R.; Yang, Y.; Santambrogio, G.; Brümmer, M.; Roscioli, J. R.; McCunn, L. R.; Johnson, M. A.; Kühn, O. *Angew. Chem. Int. Ed.* **2007**, *46*, 8691–8694. (f) Goebbert, D. J.; Santambrogio, G.; Yang, Y.; Kühn, O.; Meijer, G.; Asmis, K. R., submitted for publication.
(4) Day, V.; Alamgir Hossain, M.; Kang, S. O.; Powell, D.; Lushington, G.; Bowman-James, K. *J. Am. Chem. Soc.* **2007**, *129*, 8692–8693.
(5) (a) Alder, R. W. *Chem. Rev.* **1996**, *96*, 2097–2111. (b) Alder, R. W. *J. Am. Chem. Soc.* **2005**, *127*, 7924–7931. (c) Mascal, M.; Lera, M.; Blake, A. J.; Czaja, M.; Kozak, A.; Makowski, M.; Chmurzynski, L. *Angew. Chem., Int. Ed.* **2001**, *40*, 3696–3608.
(6) Kiran Kumar, M.; Srinivasa Rao, J.; Prabakar, S.; Vairamani, M.; Narahari Sastry, G. *Chem. Commun.* **2005**, 1420–1422.
(7) (a) Perrin, C. L.; Nielson, J. B. *Annu. Rev. Phys. Chem.* **1997**, *48*, 511–544. (b) Perrin, C. L.; Ohta, B. K. *J. Am. Chem. Soc.* **2001**, *123*, 6520–6526. (c) Perrin, C. L.; Ohta, B. K. *J. Mol. Struct.* **2003**, *644*, 1–12. (d) Bienko, A. J.; Łatajka, Z.; Sawka-Dobrowolska, W.; Sobczyk, L.; Ozeryanskii, V. A.; Pozharskii, A. F. *J. Chem. Phys.* **2003**, *119*, 4313–4319.
(8) Poutsma, J. C.; Andriole, E. J.; Sissung, T.; Morton, T. H. *Chem. Commun.* **2003**, 2040–2041.
(9) (a) Masri, F. N.; Wood, J. L. *J. Mol. Struct.* **1972**, *14*, 217–227. (b) Morton, T. H.; Beauchamp, J. L. *J. Am. Chem. Soc.* **1972**, *94*, 3671–3672. (c) Howard, S. T.; Platts, J. A.; Alder, R. W. *J. Org. Chem.* **1995**, *60*, 6085–6090. (d) Meot-Ner, M. *Chem. Rev.* **2005**, *105*, 213–284. (e) Rõõm, E.-I.; Kütt, A.; Kaljurand, I.; Koppel, I.; Leito, I.; Koppel, I. A.; Mishima, M.; Goto, K.; Miyahara, Y. *Chem.—Eur. J.* **2007**, *13*, 7631–7643.
(10) Antony, J.; Grimme, S. *J. Phys. Chem. A* **2007**, *111*, 4862–4868.
(11) (a) Munowitz, M. G.; Griffin, R. G. *J. Chem. Phys.* **1982**, *76*, 2848–2458. (b) Song, X.-J.; Rienstra, C. M.; McDermott, A. E. *Magn. Reson. Chem.* **1981**, *39*, S30–S36. (c) Zhao, X.; Sudmeier, J. L.; Bachovchin, W. W.; Levitt, M. H. *J. Am. Chem. Soc.* **2001**, *123*, 11097–11098.
(12) Pietrzak, M.; Try, A. C.; Andrioletti, B.; Sessler, J. L.; Anzenbacher, P., Jr.; Limbach, H.-H. *Angew. Chem., Int. Ed.* **2008**, *47*, 1123–1125.
(13) Herzfeld, J.; Berger, A. E. *J. Chem. Phys.* **1980**, *73*, 6021–6030.
(14) (a) Zilm, K. W.; Grant, D. M. *J. Am. Chem. Soc.* **1981**, *103*, 2913–2922. (b) Anderson-Altmann, K. L.; Phung, C. G.; Mavromoustakos, S.; Zheng, Z.; Facelli, J. C.; Poulter, C. D.; Grant, D. M. *J. Phys. Chem.* **1995**, *99*, 10454–10458. (c) Harris, R. K.; Packer, K. J.; Thayer, A. M. *J. Magn. Reson.* **1985**, *62*, 284–297. (d) Wu, G.; Wasylishen, R. E.; Power, W. P.; Baccolini, G. *Can. J. Chem.* **1992**, *70*, 1229–1235.
(15) Ishii, Y.; Terao, T.; Hayashi, S. *J. Chem. Phys.* **1997**, *107*, 2760–2774.
(16) Aristotle (*On the Heavens* II.xiii.295b.31−34) does not clearly specify whether man or beast, but later writers have supposed it to be a donkey.
(17) (a) Kreevoy, M. M.; Liang, T. M. *J. Am. Chem. Soc.* **1980**, *102*, 3315–3322. (b) Frey, P. A.; Cleland, W. W. *Bioorg. Chem.* **1998**, *26*, 175–192. (c) Hud, N.; Morton, T. H. *J. Phys. Chem. A.* **2007**, *111*, 3369–3377.

JA8018725